analytical chemistry

pubs.acs.org/ac Article

Enhanced Spatial Proteomics and Metabolomics from a Single Tissue Section Using MALDI-MSI and LCM-microPOTS Platforms

Marija Veličković, Le Z. Day, Kevin J. Zemaitis, Isaac Kwame Attah, Kristin E. Burnum-Johnson, Christopher R. Anderton, and Dušan Veličković*

Cite This: https://doi.org/10.1021/acs.analchem.5c05005 Read Online

ACCESS | Metrics & More | Article Recommendations | Supporting Information

ABSTRACT: Spatially resolved mass spectrometry (MS)-based multiomics workflows are becoming more utilized for revealing the complex biology that occurs within tissues. However, these approaches commonly require multiple independent tissue sections to analyze the metabolite and protein compositions of these samples. This poses a significant challenge in preserving cell- or region-specific molecular fidelity, as variations between tissue sections can compromise the accurate correlation of molecular data. Here, we developed workflows for comprehensive multiomics profiling from a single tissue section (STS) using different MS modalities. We enhanced the functionality of an electrically insulated substrate by employing metal-assisted approaches that enabled both MS-based untargeted spatial metabolomics and proteomics from STS. This allowed metabolite imaging using matrix-assisted laser desorption/ionization-MS imaging (MALDI-MSI), without compromising it for subsequent proteome profiling with laser capture microdissection (LCM)-based technology. Specifically, implementing copper tape as a backing for polyethylene naphthalate (PEN) slides enabled the detection of >140 metabolites across a poplar root tissue section using MALDI-trapped ion mobility spectrometry time-of-flight (timsTOF)-MS. Afterward, we detected 6571 unique proteins from two distinct root regions by leveraging LCM technology coupled to our microdroplet based sample preparation approach. We also developed an alternative workflow utilizing gold-coated PEN substrates for imaging with MALDI-Fourier-transform ion cyclotron resonance (FTICR)-MS, which permitted the profiling of >170 metabolites and the identification of 6542 unique proteins across a single poplar root tissue section. These results were comparable to using each omics analysis independently. These approaches offer new opportunities for high-resolution molecular profiling of multiple omics levels across biological tissues.

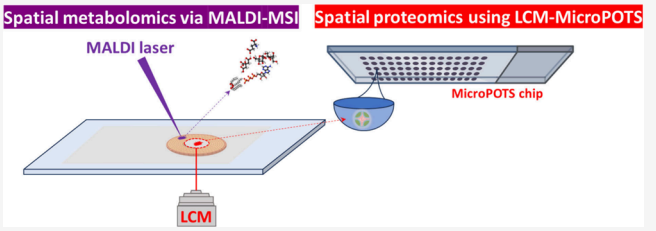

INTRODUCTION

The molecular landscapes in biological tissues are highly diverse and heterogeneous, primarily due to the presence of various cell types and unique microenvironments.[1] Mass spectrometry (MS)-based omics techniques are widely used for comprehensive assessments of different classes of biological molecules (e.g., proteins,[2] glycans,[3] lipids,[4] and metabolites[5]), advancing our understanding of molecular complexity of biological tissues.[6,7] Incorporation of the spatial dimension into MS-based omics data has offered new ways of understanding tissue biology by uncovering underlying molecular signatures that map cellular diversity and delineate functional heterogeneity within the tissue. For example, MS imaging (MSI) has been a powerful technique to study the molecular composition within the full spatial context of tissue microenvironments. This technique enables untargeted in situ analysis, capturing molecular snapshots of biological processes across and throughout biological tissues.[8−11]

Each omics approach reflects only a subset of the biochemical processes within a sample and cannot capture the complexity of molecular events and the interactions biomolecules are involved in.[6] In contrast, data combined from multiple omics levels can provide a more holistic and comprehensive perspective of the molecular cascades that occur within tissues.[12] Thus, cross-omics integrative approaches are crucial for achieving a more comprehensive overview of biological processes and an in-depth understanding of biological activities at a systemic level.[13−15] Consequently, increasing attention has been focused on developing MSI workflows that enable multiomics characterization of specific cell types or regions with the full spatial context of the tissue microenvironment.[16]

Previous efforts have used a single matrix-assisted laser desorption/ionization (MALDI)-MSI modality to profile multiple omics levels on a single tissue section (STS), which facilitated enhanced molecular characterization through the

Received: August 14, 2025
Revised: October 16, 2025
Accepted: October 20, 2025

integration of cross-omics data.[17,18] While MALDI-MSI is a powerful technique for metabolite and lipid imaging, comprehensive proteome imaging by MALDI-MSI remains a challenge. This limitation arises due to MALDI's tendency to generate primarily singly charged ions, which do not yield as informative MS/MS data as multiple charged ions. Additionally, challenges such as ion suppression due to the effect of the biological matrix and the lack of separation make MALDI imaging of proteins difficult and unpopular. Although protein coverage can be improved with on-tissue digestion, in situ MS/MS peptide identification remains challenging due to low signal-to-noise ratios and high spectral complexity that impede database identifications.[15]

Alternative approaches for spatial proteome analysis, often using laser capture microdissection (LCM), are becoming increasingly employed. However, integrating MALDI-MSI and LCM-based approaches for advanced molecular characterization necessitates the use of sequential tissue sections for optimal data from both methods. This is because different MS-modalities demand specific sample handling and preparation methods, including the types of slides on which the samples are mounted. This dependence on separate tissue sections for multiomics profiling hinders the ability to profile the same microanatomical regions or individual cellsacross different molecular imaging techniques. This is particularly evident in highly heterogeneous samples, where certain cell types may be confined to a single tissue layer, making consecutive sections distinctly different in composition.

Our previously published Metabolome Informed Proteome Imaging (MIPI) workflow exemplifies this requirement.[14,15] MIPI requires tissue sections to be mounted on conductive indium tin oxide (ITO)-coated slides for lipidomic and metabolomic profiling by MALDI-MSI, ensuring efficient ion transfer and a uniform signal across the entire tissue section. For the downstream LCM-based proteomic profiling, tissue sections must be mounted on PEN-membrane slides to facilitate region-specific cell collection using an ultraviolet (UV) LCM system that is seamlessly combined with microdroplet processing in one pot for trace samples (microPOTS) technology. A combination of these two techniques can enable multimodality to achieve enhanced molecular characterization from an STS, and there has been huge effort of the analytical community to achieve this goal.[19−22] Nevertheless, there is a notable analytical challenge of substrate requirements. Several previous efforts have aimed to address this issue and used the same tissue section for imaging with different modalities.[23−26] For example, Dilillo et al. utilized atmospheric pressure (AP) MALDI for imaging from a nonconducive PEN slide, following the more in-depth molecular profiling by the LCM-based approach.[24] While AP-MALDI-MSI enables routine analysis on electrically insulating samples, its sensitivity and metabolite coverage were noticeably reduced in comparison to conventional vacuum MALDI-MSI.[27] Alternatively, Mezger et al. employed UV ablation for MSI-guided proteomics from a single conductive slide, where the tissue section was directly mounted on the ITO-coated slide instead of a PEN membrane.[25] Although this method is feasible and practical, the reported proteome coverage from ITO slides was significantly lower than the coverage obtained from PEN membrane slides for both frozen and formalin-fixed paraffin-embedded (FFPE) tissue samples. Additionally, another report found that UV ablation using the LCM instrument had lower reproducibility, even under the optimized conditions, potentially due to its strong dependence on the characteristics of the biological surface being sampled.[26] Hendriks at al. presented an innovative MALDI-MSI-guided liquid chromatography (LC)-MS/MS lipidomics and proteomics workflow from a single section of glioblastoma multiforme brain tumor.[41] They assessed the influence of different slide types (i.e., PEN, ITO, and IntelliSlides) for downstream proteomics and lipidomics analyses, but the corresponding MALDI-MSI data and identity of lipids detected by MALDI-MSI from PEN and other slide types were not evaluated. The feasibility of performing MALDI-MSI using nonconductive substrates was also investigated by other groups, along with exploring the potential for enhancing signal intensity through the addition of metal.[28−33]

Herein, we demonstrate enhancement of the functionality of an electrically insulative PEN substrate to more optimally enable its application for MALDI-MSI followed by LCM-based proteomics. This resulted in efficient and reproducible untargeted spatial metabolomics and untargeted spatial proteomics workflows from a STS. We optimized PEN-mounted slides for MALDI analysis on both trapped ion mobility time-of-flight (timsTOF)-MS and Fourier-transform ion cyclotron resonance (FTICR)-MS instrument platforms using several slide preparation procedures, including backing the PEN slide with copper (Cu) tape and sputtering gold (Au) for increasing conductivity. We additionally evaluated how these sample preparations and MALDI-MSI analysis affected downstream proteomic analyses, and we compared these results to each omics analysis performed independently.

EXPERIMENTAL SECTION

Plant Growth and Harvesting. Nisqually-1 cuttings were used in this study. Small cuts (approximately 5−8 in.) were made from stock (mother) plants maintained in a Conviron walk-in growth chamber at 24 °C (16 h per day/8 h per night) with a light intensity of 400 μM/sec. The stem base of cuttings was treated with commercially available rooting powder (Rhizopon AA#2, Hortus USA Corp., NY, USA) and planted in soil pots (4 in. square pots) to enable the rooting process. Small stem cuttings were grown under plant growth conditions similar to those described above. After 21 days, the stem cuts were checked for newly formed roots and then transplanted onto bigger soil pots (4 in. × 4 in. × 9.5 in.) containing Pro-mix BX soil and fertilized. The cuts were allowed to establish root system in another 2 weeks until harvesting. The entire root system was gently and quickly soaked and washed with water; the primary (longest) root was excised from the stem in a mixture of 7.5% hydroxypropyl methylcellulose (HPMC) and 2.5% polyvinyl-pyrrolidone (PVP) and then snap froze the sample in isopropanol chilled on dry ice and stored the tissue at −80 °C. For the first demonstration of our MIPI-STS workflow, we used freshly harvested samples. For demonstration of alternative workflow that utilized gold coating, we used old poplar root that was embedded in HPMC with PVP and stored at −80 °C for two years.

Cryosectioning. The embedded samples were cut into 10 μm thick sections using a CryoStar NX70 (Thermo Fisher) with a blade temperature of −14 °C and specimen temperature of −16 °C. Replicate sections were thaw-mounted onto PEN slides (ZEISS) and ITO slides (Bruker Daltonics), dried under vacuum, and stored at −80 °C in vacuum-sealed bags with desiccant until analyzed.

MALDI Matrix Spraying Protocols. An M5 Sprayer (HTX Technologies, Chapel Hill, NC) was used for the application of

https://doi.org/10.1021/acs.analchem.5c05005
Anal. Chem. XXXX, XXX, XXX−XXX

all matrices and on-target chemical derivatization (OTCD) agents.

For OTCD in positive ion mode, aqueous solutions of 6 mg/mL 1-ethyl-3-(3-(dimethylamino)propyl)carbodiimide (EDC) and 2 mg/mL 4-(2-((4-bromophenethyl)dimethylammonio)-ethoxy)benzenaminium bromide (4-APEBA) were sprayed consecutively using the same parameters: 25 μL/min flow rate, a nozzle temperature of 37.5 °C, four cycles at 3 mm track spacing with a crisscross pattern, a 2 s drying period, 1200 mm/min spray head velocity, and 10 PSI of nitrogen gas. Immediately after EDC and 4-APEBA application, the M5 Sprayer was used to spray the MALDI matrix with 2,5-dihydroxybenzoic acid (DHB) (Fisher Chemical; Fair Lawn, NJ). DHB was prepared at a 40 mg/mL concentration in 70% MeOH and sprayed at 50 μL/min flow rate. The nozzle temperature was set to 70 °C, with 12 cycles at 3 mm track spacing with a crisscross pattern. A 2 s drying period was added between cycles, and a linear flow was set to 1200 mm/min with 10 PSI of nitrogen gas. This resulted in matrix coverage of ∼667 μg/cm^2 for DHB.

For negative ion mode, naphthyl ethylenediamine dihydrochloride (NEDC) was prepared at a concentration of 7 mg/mL in 70% MeOH and sprayed at a 120 μL/min flow rate. The nozzle temperature was set to 70 °C, with eight cycles at 3 mm track spacing in a crisscross pattern without a drying period between cycles. A linear flow was set to 1200 mm/min with 10 PSI nitrogen gas and a 40 mm nozzle height. This resulted in matrix coverage of ∼187 μg/cm^2 for NEDC.

Gold (Au) Coating Protocol. For our alternative workflow that utilized gold coating for MALDI-MSI on the FTICR, Au was coated over a PEN slide with a NEDC matrix. PEN slide was fixed on a tilted rotary stage within a Cressington HR 208 (Watford, UK) sputter coater loaded with a 0.5 mm gold target (4N, Espi Metals, Ashland, OR). The chamber was adjusted to 0.1 mbar, the sample stage was rotated at maximum speed, and sputtering of a 10 nm layer of gold was completed at 20 mA controlled by a Cressington MTM-20 (Watford, UK) thickness controller over the course of several minutes. A flatbed scanned image of Au-coated slide is provided in Figure S1.

MALDI-timsTOF-MSI Analyses. Slides were mounted either on a polished steel MTP PAC adapter (Bruker Daltonics) by securing the slide with doubled-sided copper tape (3-6-1182; 3 M USA) or on an MTP Slide Adapter II (Bruker Daltonics), designed to accommodate 75 mm × 25 mm glass slides.

Analyses were performed on a timsTOF Flex, equipped with a SmartBeam 3D (355 nm) Nd: YAG laser (Bruker Daltonics). The instrument was calibrated using an Agilent Technologies ESI-L Low Concentration Calibration Standard Tuning Mix. For OTCD/positive ion mode analysis, the instrument collected ions from m/z 200 to 1200, with 1 burst of 200 shots per pixel at frequency of 10 kHz. For negative ion mode, the instrument was operated to collect ions from m/z 50 to 650 with 1 burst of 400 shots at a frequency of 10 kHz. The step size for all analyzes was 20 μm, using "Single" smart beam setting, with 16 μm scan range, and resulting field size 20 μm, and TIMS was off. For each tissue section, the Z Position was manually adjusted so that the difference in height at the current position was within ±1 μm.

MALDI-FTICR-MSI Analyses. Analyses were performed on a 12T solariX FTICR MS, equipped with a ParaCell and an Apollo II ESI and MALDI source with a 2 kHz SmartBeam II frequency-tripled (355 nm) Nd:YAG laser (Bruker Daltonics, Bremen, Germany).

For OTCD analyses, the acquisition methods used a lock mass to the molecular ion of $[\text{APEBA-H}_2\text{O}]^+$ ($C_{18}H_{24}N_2OBr$) at m/z 363.10665. All spectra were acquired in positive ion mode, with broadband acquisition from m/z 147.42 to 1000.00 with a file size of 2 million points per spectrum (2M), at 1000 Hz, and acquisitions resulted in recording of 0.8389 s transients with 100 laser shots per pixel using default small focus and a smart walk pattern of 25 μm. This resulted in an estimated mass resolving power of ∼190,000 at m/z 400.

For NEDC sprayed slides, the acquisition method used lock mass to the NEDC peak at m/z 256.77695. All spectra were acquired in the negative ionization mode, with broadband acquisition from m/z 98.3 to 1100.00 with a file size of 2M, at 1000 Hz, with 200 laser shots per pixel using default small focus and a smart walk pattern of 25 μm. This resulted in an estimated mass resolving power of ∼130,000 at m/z 400.

MALDI MSI Data Processing, Annotation, and Analysis. FTICR and timsTOF MALDI-MSI data collected with FlexImaging (Bruker Daltonics, Bremen, DE) were imported individually into SCiLS Lab (v2025a Premium 3D, Bruker Daltonics, Bremen, DE), where centroided data sets were exported to imzML for annotation by METASPACE. FTICR and timsTOF data sets were annotated with sub-3 ppm and sub-12 ppm mass error, respectively, and searched with the possible chemical modification of $[+C_{18}H_{22}N_2Br]$ for OTCD, and as $[M-H]^-$ and $[M+Cl]^-$ adducts for NEDC analyses, against the KEGG database and are reported with an FDR of ≤20%. Additionally, all annotated m/z values from FTICR data sets were imported back into SCiLS of respective timsTOF data sets, where the manual peak-by-peak inspection was performed to add timsTOF annotations that METASPACE did not pick. Only symmetrical baseline-separated peaks were taken into account. All MALDI-MSI data, annotations, and ion images reported in this manuscript can be visualized and browsed in METASPACE: https://metaspace2020.org/project/c5bf916e-6ee3-11ef-a046-5bfb2255949c?tab=datasets.

Matrix Removal and Tissue Fixation. The MALDI matrix was removed by submerging the slide in 70% methanol for 1 min, followed by fixation in a gradient of ethanol solutions (70%, 96%, and 100% ethanol, respectively) for 30 s each. The slide with tissue sections was then dried under the vacuum for 15 min. PEN slides with control tissue sections were gradually dehydrated with ethanol, as described above.

Laser Capture Microdissection (LCM). Cell-type specific populations of poplar root tissue, ranging from 150,000 to 250,000 μm^2, were excised using a PALM MicroBeam system (ZEISS) and collected in the corresponding microwells of the microPOTS chip, which were preloaded with 2 μL of DMSO to serve as a capturing medium for the excised tissue voxels. For our initial assessment of the multiomics workflow on proteome coverage, we independently collected entire region of vascular cells (V) and similarly sized region containing populations of epidermal and cortical cells (C+E) from a single tissue section. We collected replicates (n = 4) of each region of interest (ROI) from control sections and replicates (n = 3) of each ROI from post-MALDI sections analyzed on timsTOF using both OTCD and NEDC workflows.

For demonstration of alternative workflow, we separately collected three ROIs: the entire vascular (V) region, the entire cortical (C) region, and the entire epidermal (E) region from a single tissue section. We collected replicates (n = 2) of each ROI from control sections, as well as replicates (n = 2) of each ROI from post-MALDI-MSI sections coated with gold and analyzed on the FTICR. Additionally, a single replicate of each ROI was collected from post-MALDI sections analyzed by timsTOF,

https://doi.org/10.1021/acs.analchem.5c05005
Anal. Chem. XXXX, XXX, XXX−XXX

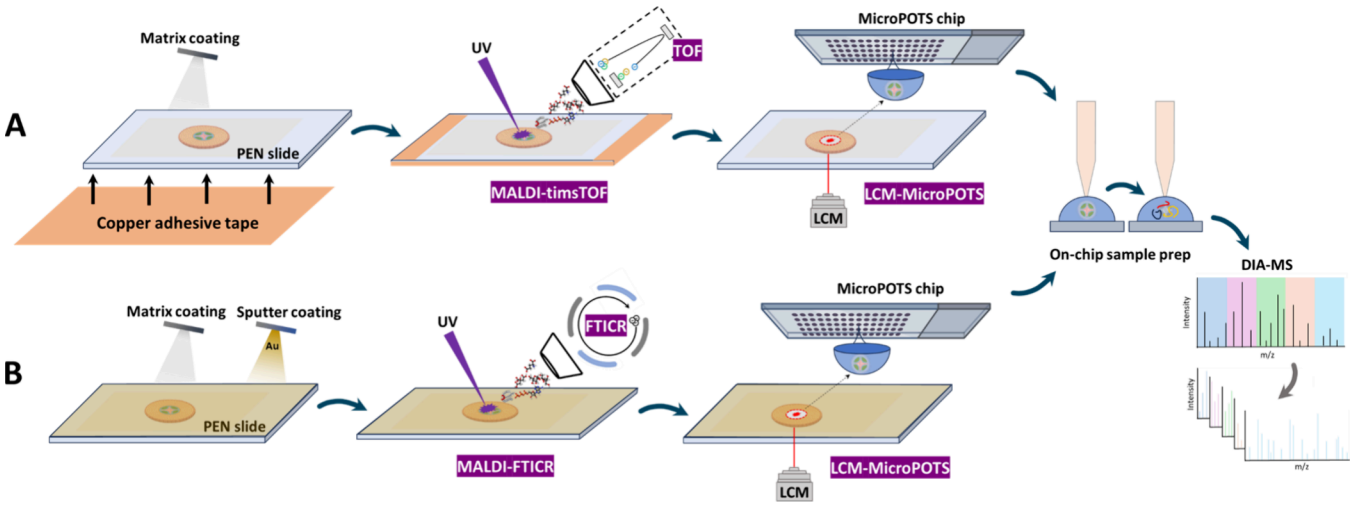

Figure 1. Two alternative strategies of the advanced MIPI approach that combine two complementary microscale spatial modalities for metabolomics and proteomics analyses from a single tissue section. (A) Overview of the workflow that utilizes Cu-tape back-coated PEN slide for MALDI imaging using timsTOF instrument and downstream proteome profiling using LCM-microPOTS approach. (B) Overview of the workflow that utilizes a PEN slide with MALDI matrix and coated Au for MALDI imaging using an FTICR instrument and subsequent proteomics analysis utilizing LCM-microPOTS approach.

since this condition had been previously assessed in our earlier experiments.

Proteomics Sample Processing in a Microdroplet and LC-MS/MS Peptide Analysis. Sample processing was carried out on chip using a previously published manual pipetting protocol.[15] The microPOTS chip and its cover were incubated at 75 °C for 1 h to dry the DMSO solvent. Next, 2 μL of extraction buffer containing 0.1% DDM, 0.5 × PBS, 50 mM TEAB, and 1 mM DTT was dispensed into each well of the chip. The chip was incubated at 75 °C for 1 h. Thereafter, 0.5 μL of IAA solution (10 mM IAA in 100 mM TEAB) was added to the corresponding wells with the samples, followed by incubation at room temperature for 30 min. All samples were subsequently digested by adding 0.5 μL of an enzyme mixture (10 ng of Lys-C and 40 ng of trypsin in 100 mM TEAB) and incubating at 37 °C for 10 h. Following digestion, peptides were acidified by adding 5% FA to each sample to a final concentration of 1% FA. Each sample was collected and dispensed into a 4 μL aliquot of LC buffer A (water with 0.1% FA), centrifuged at 10,000 *g* for 5 min at 25 °C, and transferred (~7.5 μL) to an autosampler vial coated with 0.01% DDM. To minimize droplet evaporation, during every manipulation of the sample, the microPOTS chip was placed on an ice pack. Also, during each incubation, the microPOTS chip was sealed with the chip cover, wrapped in aluminum foil, and incubated in a humidified chamber.

Liquid chromatography separation was performed using a Vanquish Neo LC (Thermo Scientific), running a 70 SPD (samples per day) separation method with each sample run having a 14 min active gradient and 6 min for sample loading and column equilibration. The Vanquish Neo was configured to run in trap-and-elute mode, utilizing the PepMap Neo Trap Cartridge (Thermo Scientific) for sample trapping and reverse flow unto the analytical column. A PepMap ES906 analytical column (Thermo Scientific) was used for the reverse phase elution of the peptides. The gradient method used for the separation is detailed in Table S1. The analytical column was interfaced to an Orbitrap Astral mass spectrometer (Thermo Scientific) by using an EASY-Spray source. The ion source conditions were 2.2 kV and 300 °C for the spray voltage and Ion transfer tube temperature, respectively.

For MS analysis, full scan spectra were acquired using the Orbitrap analyzer in the scan range of m/z 380 to 980, and at a resolution of 240,000. The normalized AGC target was set at 500%, with a maximum injection time at 5 ms, and the RF lens was set at 45%. For nDIA acquisition, data was acquired in the mass range of m/z 380 to 980, DIA window type set to "Auto", window placement optimization set to "On", window overlap set at 0, and isolation window set at 2 m/z. Higher-energy collisional dissociation was performed at a normalized collision energy of 25%, and the scan range was set to m/z 150 to 2000. RF lens was set at 40%, AGC target set to "Custom", normalized AGC target set at 500%, and the maximum injection time was set at 3 ms. Loop control was set at 0.6 s.

The proteomic data raw files were processed by DIA-NN (version 1.9.2)[34] and searched against the *Populus trichocarpa* UniProt protein sequence database (UP000006729, accessed 03/2018). The search settings included FASTA digest for library-free search/library generation, deep learning-based spectra, RTs and IMs prediction, and trypsin as the protease with allowance for one missed cleavage. Carbamidomethylation was set as a fixed modification, and variable modifications included oxidation of methionine and N-terminal acetylation. Match between runs was enabled, and protein inference was grouped on genes. Machine learning utilized the single-pass NNs mode, and quantification utilized a high precision strategy. The cross-run normalization was set as RT-dependent, and library profiling employed smart profiling techniques. The remaining parameters were kept as the default settings for this analysis.

Data are available through MassIVE (https://massive.ucsd.edu), a full partner of ProteomeXchange, through the following database accession: MSV000098730; password: Tissue6833.

RESULTS AND DISCUSSION

Herein, we integrated two complementary MS-based spatial modalities to achieve cross-omics molecular profiling from a STS. Our newly developed MIPI-STS addresses key challenges

https://doi.org/10.1021/acs.analchem.5c05005
Anal. Chem. XXXX, XXX, XXX−XXX

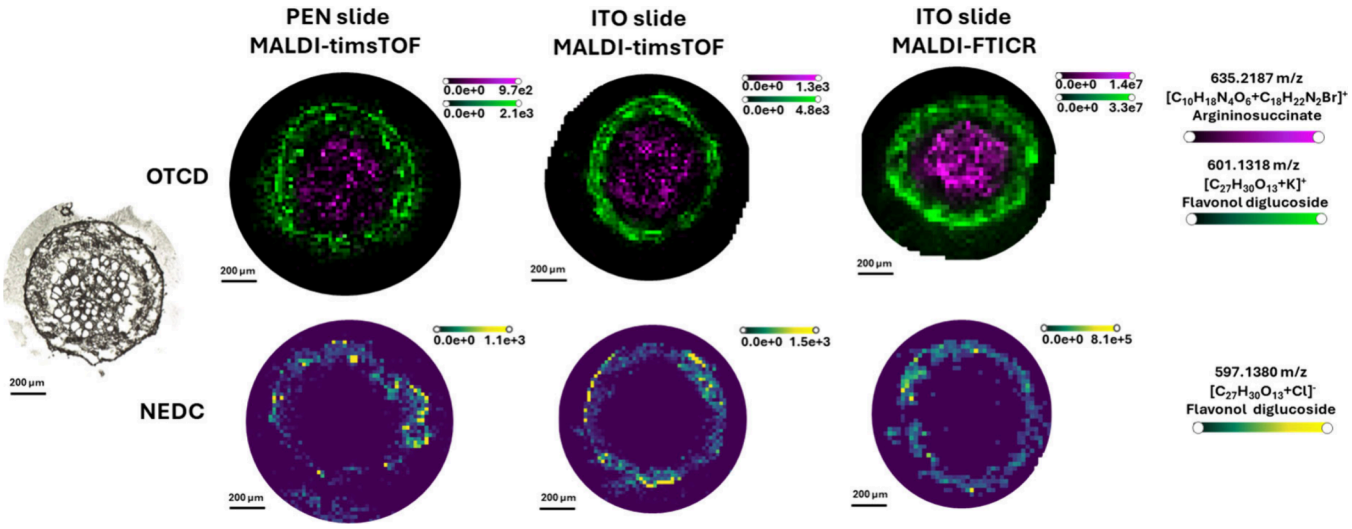

Figure 2. Example ion images of flavonol diglucoside and argininosuccinate, demonstrating consistent spatial distribution across varying experimental conditions. These include substrates (PEN and ITO slides) and workflows (NEDC and OTCD), with corresponding signal intensities captured using timsTOF and FTICR. The microscopy image of a 10 μm thick poplar root cryosection.

associated with the need for serial sections and substrate incompatibilities between the modalities (i.e., MALDI-MSI and LCM-based spatial MS). Based on previously reported MALDI-MSI analysis from nonconductive substrates, we developed two MIPI-STS workflows, which can be adapted based on the specific MALDI instruments available in the lab. Implementation of a conductive copper tape adhesive approach onto an insulated substrate that is suitable for LCM-based MSI allowed us to achieve MALDI-timsTOF data quality matching to the data quality from ITO slides (Figure 1A). Alternatively, the gold coating approach was employed for MALDI imaging on the FTICR, utilizing a substrate that remains compatible with the downstream LCM-microPOTS pipeline for proteome profiling (Figure 1B). As such, we overcame the difficulties of combining MALDI-MSI and LCM-based MSI for comprehensible multiomics characterization from an STS. To benchmark our approach, we utilized poplar root tissue, since we already demonstrated cell-specific metabolic activities using MALDI-MSI in this system, accompanied by the internal database generated using MALDI-FTICR.[35] While MIPI-STS is specifically designed for the characterization of highly heterogeneous samples, for workflow development and assessments, we used poplar root tissues due to their minimal section-to-section variation. This choice allowed us to perform multiple analyses and establish robust controls, enabling accurate comparisons and assessments that would otherwise be difficult with highly heterogeneous samples.

MIPI-STS Workflow for Metabolomic Imaging by MALDI-timsTOF and Downstream LCM-microPOTS Proteomics Analysis. Figure 1A depicts our MIPI-STS workflow with a PEN membrane slide and the timsTOF data acquisition. A 10 μm thick cryosection of the embedded poplar root tissue was placed on a PEN slide. The back side of the slide was covered with copper tape and analyzed using MALDI-MSI for spatial metabolomics to visualize metabolites across different cell regions and identify areas of interest for subsequent proteomics. Post-MALDI-MSI sections were washed for matrix removal and subjected to LCM-based spatial proteomics leveraging our microPOTS approach to profile enzymes from the mapped regions.

To establish an effective MALDI-MSI protocol, we evaluated different chemical matrices for imaging the metabolome of poplar root tissue. Specifically, we tested two commonly used MALDI matrices in our laboratory for plant metabolomics imaging: NEDC and DHB were used for negative and positive ion mode imaging, respectively, with an important note that OTCD was performed before spraying the DHB matrix. We previously showed that OTCD using EDC and 4-APEBA derivatization agents enhance sensitivity and expand coverage of carbonyl phytocompounds,[35] therefore we incorporated it into our workflow. Metabolomic imaging results were benchmarked by comparing them to the results obtained using traditional conductive ITO-coated glass slides in a standard MTP slide holder.

Since the used PEN slide was dimensionally incompatible with the commercially available Bruker MTP slide holder, our initial experimental setup involved securing the PEN slide onto an MTP PAC adapter. Our initial metabolomic imaging on MALDI-timsTOF from PEN slide secured on the MTP PAC adapter yielded comparable results using both matrices, DHB-OTCD and NEDC, relative to control sections on ITO slides. The use of the NEDC matrix resulted in annotation of an identical number of features (~210) on PEN and ITO slides (Table S4). It also showed high repeatability annotation- and intensity-wise (Figure S2). Similarly, the OTCD workflow with the DHB matrix provided consistent performance across sections on PEN and ITO slides, each detecting ~140 annotated features. In terms of metabolome coverage, a total of 62 metabolites overlapped between the NEDC and OTCD workflows, while other metabolites were unique for each workflow, reflecting their differing specificities, which is consistent with our previous findings regarding the distinct analytical profiles of the two approaches.[35] MALDI-MSI using the 4-APEBA OTCD workflow effectively captures both derivatized and underivatized molecules, as depicted in Figure 2. For instance, argininosuccinate, an intermediate in the arginine biosynthesis pathway, was detected in the vascular region, and it was captured in its derivatized form. On the other hand, flavonol diglucoside was captured in its endogenous, underivatized form, showing accumulation in the cortex with

https://doi.org/10.1021/acs.analchem.5c05005
Anal. Chem. XXXX, XXX, XXX−XXX

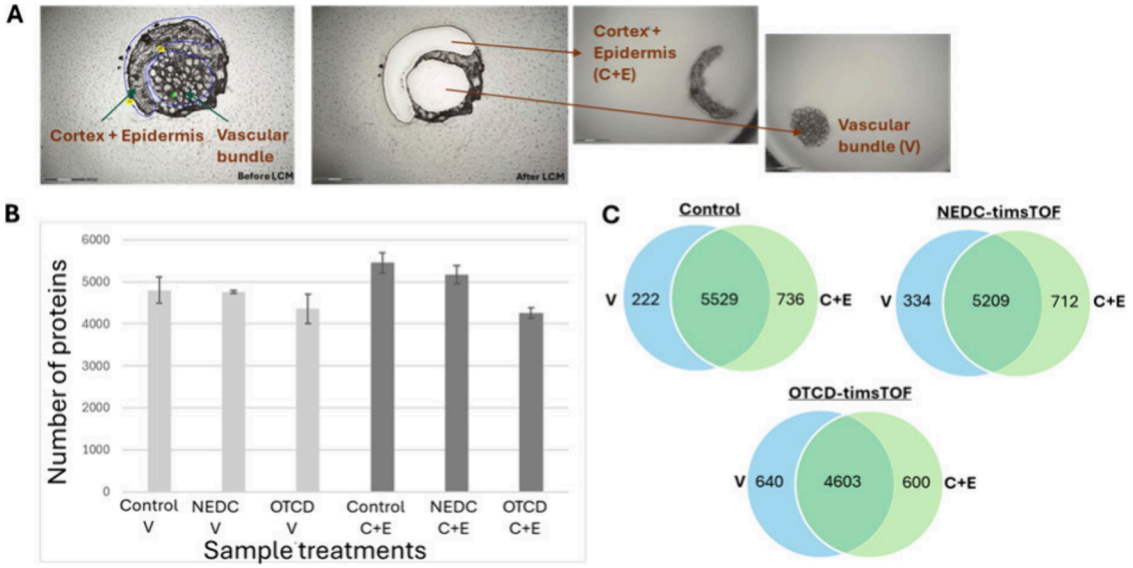

Figure 3. Profiling of region-specific enzymes using LCM-microPOTS processing. (A) LCM collection of microscale regions from MALDI-imaged sections analyzed by timsTOF. (B) Bar graph depicting the effect of MALDI-MSI analysis on proteome coverage, comparing samples obtained using NEDC and OTCD workflows and untreated control samples. (C) Venn diagram showing high overlap of proteins across V and C+E ROIs for both post-MALDI-timsTOF workflows and control samples. The number of unique proteins is counted across all replicates per condition.

notably higher abundance in the epidermis. Similar signal intensities were obtained for both metabolites when imaged from the PEN setup and the control ITO slide. By leveraging the NEDC workflow, the flavanol diglucoside was imaged with identical signal intensity and spatial localization from PEN and control ITO on the timsTOF, cross validating the reliability of our workflows. Furthermore, the imaging results showed the same spatial patterns when compared to previous imaging results obtained by FTICR from poplar root cryosections on an ITO slide, which was used for internal database curation.

Next, we visually inspected the post-MALDI tissue section to assess the sample-destructive properties of the timsTOF system across both workflows. The level of tissue ablation depends on various laser parameters (such as shot count, frequency, and laser energy),[36,37] as well as the chemistry, size, and distribution of the matrix crystals, with larger crystals requiring higher laser power for ionization compared to smaller crystals.[38] Nonetheless, both workflows demonstrated their effectiveness in enabling minimal destructive sampling, thereby preserving the integrity of the sample (Figure S3).

To assess the effect of MALDI-MSI on subsequent spatial proteome analysis, we microdissected metabolome-informed tissue regions from post-MALDI-MSI sections on PEN slides analyzed on the timsTOF. As depicted in Figure 3A, we independently collected entire regions of vascular cells (V) from replicate sections along with replicates of similarly sized regions containing populations of cortical and epidermal cells (C+E). As a control, we collected replicate ROIs from serial sections that were not subjected to the MALDI-MSI metabolomics workflow. All samples were then processed utilizing our microPOTS approach, which allowed us to detect more than 6500 proteins (listed in Table S2) across all samples. Figure 3B shows the number of identified proteins detected across the replicates with error bars indicating the standard deviation of replicate measurements. As indicated in Figure 3B, the number of proteins between samples collected from the control slide and the PEN slide with the NEDC matrix analyzed by MALDI-MSI was very similar, while the number of identified proteins from the PEN slide with OTCD treatment was lower. Among the identified proteins, >91% in the V ROI and >92% in the C+E ROI overlapped between the NEDC workflow and the control, while >88% in the V ROI and >82% in the C+E ROI overlapped between the OTCD workflow when compared to the control. This implies that MALDI-MSI and subsequent washing procedures have a negligible impact on protein coverage in downstream proteomics analysis. The slightly lower protein coverage observed with the OTCD workflow is likely due to the use of EDC, a zero-length carbodiimide cross-linker, which may impair trypsin digestion and lead to mismatches during protein identification. Notably, a significant overlap in detected proteins was observed between the V and C+E regions (Figure 3C). This highlights the potential of a cross-omics integrative approach to uncover active pathways and metabolic conversions with greater precision at a specific time point. For instance, while argininosuccinate lyase (an enzyme critical for root elongation and overall plant growth due to its role in catalyzing the breakdown of argininosuccinate into arginine and fumarate) was detected in both V and C+E regions across all samples, metabolomics integration indicates that active conversion is occurring exclusively in the V region at that specific time point, as depicted in Figure 2.

Alternative MIPI-STS Workflow for Metabolomic Imaging by MALDI-FTICR and Downstream LCM-microPOTS Proteomics Analysis. Our initial experiment successfully demonstrated the feasibility of obtaining cross-omics data from poplar root tissue using a single tissue section while retaining the sensitivity of all modalities. Although MALDI-timsTOF demonstrated promising results for imaging on nonconductive slides, the necessity for manual data processing due to the limited mass resolution and the inability of METASPACE to reliably annotate features in timsTOF-generated data pose a challenge and can introduce ambiguity.[35] To address this, we aimed to enhance the workflow by employing metabolic imaging using the 12T-FTICR instrument, which is a gold standard for untargeted spatial metabolomics, offering much higher mass resolving power and mass accuracy in

https://doi.org/10.1021/acs.analchem.5c05005
Anal. Chem. XXXX, XXX, XXX−XXX

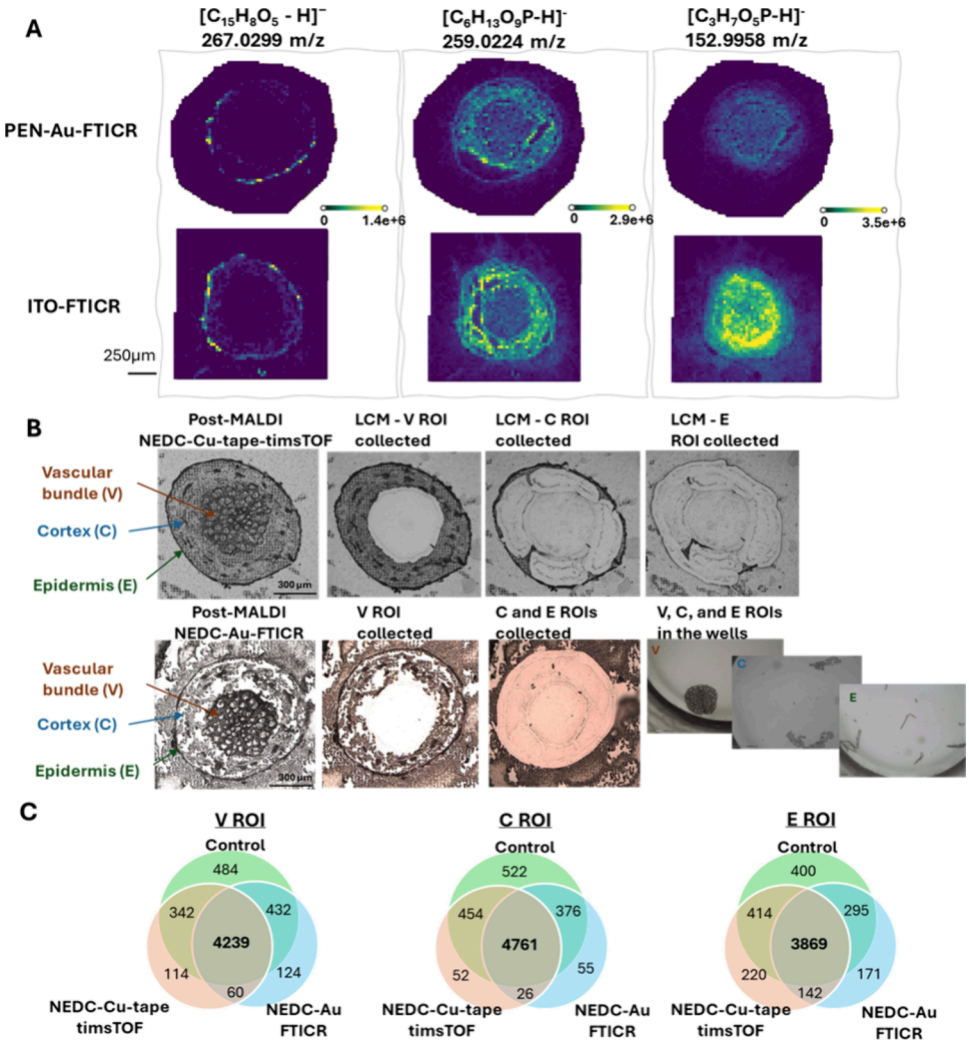

Figure 4. Profiling of region-specific enzymes using LCM-microPOTS processing. (A) Example ion image of metabolites demonstrating consistent spatial distribution and signal intensities obtained from Au-coated PEN slide and control ITO slide by MALDI-FTICR. Color bars for each m/z ion image pair (two types of slides) are placed at the same intensity scale. (B) Microscopy images of LCM-collected regions from poplar root sections after MALDI analysis, utilizing the PEN slide with a Cu-tape approach for timsTOF imaging and the PEN slide with Au-coating for the FTICR instrument imaging. (C) Venn diagram showing overlap of proteins identified across samples processed using both MIPI-STS workflows (analyzed with timsTOF and FTICR instruments) and control samples, for each ROI. The number of unique proteins is counted across all replicates per condition.

comparison to the other analyzers coupled with the MALDI source.

Therefore, we conducted another imaging experiment utilizing the Cu tape approach, but in this setup, we used a PEN slide specifically sized to fit within the slide holder, alongside a control ITO slide. The PEN slide was backed with Cu tape, which was extended over the top edges, covering the area underneath the washers of the slide adapter to ensure good conductive contact between the metal adapter and the Cu-tape-backed PEN slide. Given our previous successful demonstration of the NEDC matrix for application in multiomics imaging, we employed the NEDC workflow to test MALDI-MSI on the FTICR instrument but also on timsTOF as a reference. Consistent with our first experiment, imaging on the timsTOF using the new setup provided consistent performance across sections on both PEN and ITO slides, detecting ∼160 annotated features. While the timsTOF demonstrated comparable imaging results between conductive and nonconductive slides, MALDI-12T-FTICR was significantly less effective for imaging on Cu-tape-backed PEN slides and did not provide satisfactory metabolomic coverage. Specifically, we annotated ∼40 unique features from the PEN slides compared with ∼360 unique features from control ITO slides. As an alternative, we decided to enhance the conductivity of the PEN slide and thereby improve the MSI performance on the FTICR by using some other metal-assisted approach. As such, the specially sized PEN slide was covered with NEDC matrix, following sputter-coating of a nanolayer of gold.[32] This approach allowed us to visualize metabolites across and throughout poplar root section by using MALDI-12T-FTICR. Leveraging the METASPACE annotation platform to search against KEGG, we annotated 176 metabolites (listed in Table S3) from PEN slides using NEDC and Au-coating approach, compared to the control sample on an ITO slide with the NEDC method that profiled 180 metabolites. Their overlap was ∼90%, indicating that gold-coating did not affect MALDI-MSI outputs. Moreover, comparison of the spatial patterns and signal intensities in MALDI-FTICR data between control (ITO-FTICR) and our Au-sputtered workflow revealed consistent spatial patterns of metabolites, as well as comparable signal intensities across the tested approaches, with

https://doi.org/10.1021/acs.analchem.5c05005
Anal. Chem. XXXX, XXX, XXX−XXX

only slightly higher signal intensities for control slides (1−2.6 times) (Figure 4A).

Additionally, we evaluated the sample-destructive properties of MALDI analysis in the two proposed approaches, NEDC-Au-FTICR and NEDC-Cu-tape-timsTOF, from PEN membrane slides. Notably, the gold-coated substrate from MALDI-FTICR exhibited a higher degree of sample destruction compared with the workflow employing Cu-tape on timsTOF (Figure 4B).

To assess the impact of MALDI-MSI on subsequent spatial proteome analysis, we microdissected metabolome-informed tissue regions from sections analyzed using both the timsTOF and FTICR workflows. Selected ROIs were large, distinct, and identifiable as being histologically different, allowing them to be easily outlined for subsequent LCM work. As illustrated in Figure 4B, entire regions of V, epidermal (E), and cortical (C) cells were independently collected from replicate sections analyzed via the FTICR workflow and from control sections that were not subjected to the MALDI-MSI metabolomic workflows. Additionally, we processed a single replicate of each ROI from sections analyzed using the timsTOF workflow as an additional control, given that we had already demonstrated that this workflow has an inconsequential impact on proteomic coverage.

From the excised post-MALDI and control tissue voxels, we identified over 6500 proteins across all samples (listed in Table S2). Detailed overlap of the proteins across the approaches is indicated in Figure 4C. Depending on the ROIs, between 83% and 86% of the detected proteins were shared between post-MALDI and control samples analyzed on the timsTOF. Similarly, the gold-coating approach combined with FTICR analysis demonstrated a high overlap of 83−84% (dependent on the ROI), when compared to untreated control poplar root samples. Among nonoverlapping proteins, in all cases, there were 4−10 times more proteins detected in the control compared to the post-MALDI samples. This small number of nonoverlapped proteins detected in post-MALDI samples could be ascribed to the technical variability of the LC-MS proteomics[39] as well as to the biological variance and the fact that analysis was performed on two different tissue sections, underscoring the importance of conducting MIPI on a single tissue section to accurately capture relevant processes at a specific time and location. All these together indicate that the gold-coating method, along with the applied energy of MALDI SmartBeam II laser coupled to FTICR,[40] has a negligible impact on proteome coverage.

CONCLUSION

Here, we successfully overcame the challenges of integrating two spatial MS modalities, enabling comprehensive multiomics characterization from a single tissue section. We developed two robust workflows that deliver results comparable to those of individual omics analyses performed under ideal conditions. These workflows can be easily implemented and adapted by other research laboratories depending on the availability of FTICR, timsTOF, or other instruments for MALDI imaging.

Although we demonstrated MIPI-STS workflows on plant tissue, our workflows can be applied to virtually any complex heterogeneous tissue sample, including mammalian tissue. As such, these workflows offer broad utility and significant potential for advancing multiomics research across diverse areas of biomedical and biological investigation. Future applications are expected to address not only specific scientific questions but also the potential of employing different chemical matrices, thereby further enhancing the flexibility and versatility of this workflow.

ASSOCIATED CONTENT

Supporting Information

The Supporting Information is available free of charge at https://pubs.acs.org/doi/10.1021/acs.analchem.5c05005.

The gradient method used for peptide separation; a flatbed scanned image of the analyzed slide, showing a uniform layer of gold coating applied over the NEDC matrix-covered PEN slide containing poplar root sections; replicate poplar root sections analyzed on the timsTOF, demonstrating high repeatability when imaged using a PEN slide backed with copper tape; and microscopy images of pre- and post-MALDI analysis, demonstrating minimal destructive sampling by the timsTOF using the OTCD with DHB workflow, as well as the NEDC workflow (PDF)

A list of detected proteins, a list of detected metabolites using the PEN-NEDC-Au-FTICR approach, and a list of detected metabolites using PEN-Cu-tape-timsTOF approach (XLSX)

AUTHOR INFORMATION

Corresponding Author

Dušan Veličković − *Environmental Molecular Sciences Laboratory, Pacific Northwest National Laboratory, Richland, Washington 99354, United States;* orcid.org/0000-0001-7945-9620; Phone: +1 (509) 371-7003; Email: dusan.velickovic@pnnl.gov

Authors

Marija Veličković − *Environmental Molecular Sciences Laboratory, Pacific Northwest National Laboratory, Richland, Washington 99354, United States;* orcid.org/0000-0003-3664-5719

Le Z. Day − *Environmental Molecular Sciences Laboratory, Pacific Northwest National Laboratory, Richland, Washington 99354, United States*

Kevin J. Zemaitis − *Environmental Molecular Sciences Laboratory, Pacific Northwest National Laboratory, Richland, Washington 99354, United States;* orcid.org/0000-0002-3524-9776

Isaac Kwame Attah − *Biological Sciences Division, Pacific Northwest National Laboratory, Richland, Washington 99354, United States;* orcid.org/0000-0002-9626-2069

Kristin E. Burnum-Johnson − *Environmental Molecular Sciences Laboratory, Pacific Northwest National Laboratory, Richland, Washington 99354, United States;* orcid.org/0000-0002-2722-4149

Christopher R. Anderton − *Environmental Molecular Sciences Laboratory, Pacific Northwest National Laboratory, Richland, Washington 99354, United States;* orcid.org/0000-0002-6170-1033

Complete contact information is available at: https://pubs.acs.org/10.1021/acs.analchem.5c05005

Author Contributions

D.V. conceptualized study. C.R.A. and K.B.J. provided insightful comments about the workflow development. M.V. performed sample embedding and cryosectioning. D.V. performed MALDI MSI analyses. K.J.Z. performed Au coated experiments. D.V. and

https://doi.org/10.1021/acs.analchem.5c05005
Anal. Chem. XXXX, XXX, XXX−XXX

M.V. analyzed metabolomics data. M.V. performed complementary laser microdissection and proteomics sample preparation experiments. I.K.A. analyzed the proteomics samples. L.Z.D. performed proteomics data analyses. M.V. wrote the initial draft of the manuscript. All authors contributed with their ideas and method sections to the final manuscript writing. All authors have given approval to the final version of the manuscript.

Notes

The authors declare no competing financial interest.

■ ACKNOWLEDGMENTS

The authors thank Matthew E. Monroe for uploading the data to the repository. This research was performed on a project award (https://www.osti.gov/award-doi-service/biblio/10.46936/intm.proj.2024.61353/60012581) from the Environmental Molecular Sciences Laboratory, a DOE Office of Science User Facility sponsored by the Biological and Environmental Research program under Contract DE-AC05-76RL01830.

■ REFERENCES

(1) Wu, R.; Veličković, M.; Burnum-Johnson, K. E. *Curr. Opin Biotech* **2024**, *89*, No. 103174.
(2) Messner, C. B.; Demichev, V.; Wang, Z. Y.; Hartl, J.; Kustatscher, G.; Muelleder, M.; Ralser, M. *Proteomics* **2023**, *23* (7−8), No. e2200013.
(3) Peng, W. J.; Kobeissy, F.; Mondello, S.; Barsa, C.; Mechref, Y. *Front Neurosci-Switz* **2022**, *16*, 1000179.
(4) Wu, Z.; Shon, J. C.; Liu, K. H. *J. Lifestyle Med.* **2014**, *4* (1), 17−33.
(5) Hajnajafi, K.; Iqbal, M. A. *Proteome Sci.* **2025**, *23* (1), n/a.
(6) Babu, M.; Snyder, M. *Mol. Cell Proteomics* **2023**, *22* (6), 100561.
(7) Gemperline, E.; Keller, C.; Li, L. J. *Anal. Chem.* **2016**, *88* (7), 3422−3434.
(8) Susniak, K.; Krysa, M.; Gieroba, B.; Komaniecka, I.; Sroka-Bartnicka, A. *Acta Biochim Pol* **2020**, *67* (3), 277−281.
(9) Zhang, H.; Lu, K. H.; Ebbini, M.; Huang, P.; Lu, H.; Li, L. *Npj Imaging* **2024**, *2* (1), 20.
(10) Velickovic, D.; Anderton, C. R. *Rhizosphere-Neth* **2017**, *3*, 254−258.
(11) Amstalden van Hove, E. R. A.; Smith, D. F.; Heeren, R. M. A. *J. Chromatogr A* **2010**, *1217* (25), 3946−3954.
(12) Pinu, F. R.; Beale, D. J.; Paten, A. M.; Kouremenos, K.; Swarup, S.; Schirra, H. J.; Wishart, D. *Metabolites* **2019**, *9* (4), 76.
(13) Luo, F.; Yu, Z. J.; Zhou, Q.; Huang, A. C. *Metabolites* **2022**, *12* (1), 76.
(14) Velickovic, M.; Kadam, L.; Kim, J.; Zemaitis, K. J.; Velickovic, D.; Gao, Y. Q.; Wu, R. A.; Fillmore, T. L.; Orton, D.; Williams, S. M. *Nat. Commun.* **2025**, *16* (1), n/a.
(15) Velickovic, M.; Wu, R. A.; Gao, Y. Q.; Thairu, M. W.; Velickovic, D.; Munoz, N.; Clendinen, C. S.; Bilbao, A.; Chu, R. K.; Lalli, P. M. *Nat. Chem. Biol.* **2024**, *20* (8), 1033.
(16) Velickovic, D.; Purkerson, J.; Bhotika, H.; Huyck, H.; Clair, G.; Pryhuber, G. S.; Anderton, C. *Mol. Omics* **2025**, *21* (4), 334−342.
(17) Denti, V.; Capitoli, G.; Piga, I.; Clerici, F.; Pagani, L.; Criscuolo, L.; Bindi, G.; Principi, L.; Chinello, C.; Paglia, G. *J. Proteome Res.* **2022**, *21*, 2798.
(18) Dressman, J. W.; Bayram, M. F.; Angel, P. M.; Drake, R. R.; Mehta, A. S. *Anal. Chem.* **2025**, *97* (24), 12493−12502.
(19) Patil, A. A.; Liu, Z.-X.; Chiu, Y.-P.; Lai, T. K. L.; Chou, S.-W.; Cheng, C.-Y.; Su, W.-M.; Liao, H.-T.; Agcaoili, J. B. A.; Peng, W.-P. *Talanta* **2023**, *259*, 124555.
(20) Wenzel, R. J.; Matter, U.; Schultheis, L.; Zenobi, R. *Anal. Chem.* **2005**, *77* (14), 4329−4337.
(21) Remoortere, A. v.; van Zeijl, R. J. M.; van den Oever, N.; Franck, J.; Longuespee, R.; Wisztorski, M.; Salzet, M.; Deelder, A. M.; Fournier, I.; McDonnell, L. A. *J. Am. Soc. Mass Spectrom.* **2010**, *21* (11), 1922−1929.
(22) Zemaitis, K. J.; Velickovic, D.; Kew, W.; Fort, K. L.; Reinhardt-Szyba, M.; Pamreddy, A.; Ding, Y. L.; Kaushik, D.; Sharma, K.; Makarov, A. A.; et al. *Anal. Chem.* **2022**, *94* (37), 12604−12613.
(23) Vandergrift, G. W.; Velickovic, M.; Day, L.; Gorman, B. L.; Williams, S. M.; Shrestha, B.; Anderton, C. R. *Anal. Chem.* **2025**, *97* (1), 392−400.
(24) Dilillo, M.; Pellegrini, D.; Ait-Belkacem, R.; de Graaf, E. L.; Caleo, M.; McDonnell, L. A. *J. Proteome Res.* **2017**, *16* (8), 2993−3001.
(25) Mezger, S. T. P.; Mingels, A. M. A.; Bekers, O.; Heeren, R. M. A.; Cillero-Pastor, B. *Anal. Chem.* **2021**, *93* (4), 2527−2533.
(26) Donnarumma, F.; Murray, K. K. *J. Mass Spectrom* **2016**, *51* (4), 261−268.
(27) Keller, C.; Maeda, J.; Jayaraman, D.; Chakraborty, S.; Sussman, M. R.; Harris, J. M.; Ane, J. M.; Li, L. J. *Plant Sci.* **2018**, *9*, 9.
(28) Wu, R.; Qin, L.; Chen, L. L.; Ma, R.; Chen, D. F.; Liu, H. Q.; Xu, H. L.; Guo, H.; Zhou, Y. J.; Wang, X. D. *Chem. Commun.* **2021**, *57* (82), 10707−10710.
(29) Velickovic, D.; Winkler, T.; Balasubramanian, V.; Wietsma, T.; Anderton, C. R.; Ahkami, A. H.; Zemaitis, K. *Plant Methods* **2024**, *20* (1), n/a.
(30) Vandenbosch, M.; Nauta, S. P.; Svirkova, A.; Poeze, M.; Heeren, R. M. A.; Siegel, T. P.; Cuypers, E.; Marchetti-Deschmann, M. *Anal Bioanal Chem.* **2021**, *413* (10), 2683−2694.
(31) Dufresne, M.; Patterson, N. H.; Lauzon, N.; Chaurand, P. *Adv. Cancer Res.* **2017**, *134*, 67−84.
(32) Rafols, P.; Vilalta, D.; Torres, S.; Calavia, R.; Heijs, B.; McDonnell, L. A.; Brezmes, J.; del Castillo, E.; Yanes, O.; Ramirez, N.; Correig, X. *PLoS One* **2018**, *13* (12), No. e0208908.
(33) Saigusa, D.; Saito, R.; Kawamoto, K.; Uruno, A.; Kano, K.; Shimma, S.; Aoki, J.; Yamamoto, M.; Kawamoto, T. *Mass Spectrom (Tokyo)* **2023**, *12* (1), No. A0137.
(34) Demichev, V.; Messner, C. B.; Vernardis, S. I.; Lilley, K. S.; Ralser, M. *Nat. Methods* **2020**, *17* (1), 41.
(35) Zemaitis, K. J.; Lin, V. S.; Ahkami, A. H.; Winkler, T. E.; Anderton, C. R.; Velickovic, D. *Anal. Chem.* **2023**, *95*, 12701.
(36) Shafer, C. C.; Neumann, E. K. *Front Chem.* **2024**, *12*, 12.
(37) Kaya, I.; Michno, W.; Brinet, D.; Iacone, Y.; Zanni, G.; Blennow, K.; Zetterberg, H.; Hanrieder, J. *Anal. Chem.* **2017**, *89* (8), 4685−4694.
(38) Mahamdi, T.; Serna, C. G.; Giné, R.; Rofes, J.; Mohammed, S. A.; Ràfols, P.; Correig, X.; García-Altares, M.; Hopf, C.; Iakab, S. A.; Yanes, O. *J. Am. Soc. Mass Spectrom.* **2025**, *36* (5), 1100−1110.
(39) Piehowski, P. D.; Petyuk, V. A.; Orton, D. J.; Xie, F.; Moore, R. J.; Ramirez-Restrepo, M.; Engel, A.; Lieberman, A. P.; Albin, R. L.; Camp, D. G.; et al. *J. Proteome Res.* **2013**, *12* (5), 2128−2137.
(40) Velickovic, D.; Velickovic, M.; O'Connor, C. L.; Bitzer, M.; Anderton, C. *J. Am. Soc. Mass Spectrom.* **2025**, *36* (4), 823−828.
(41) Hendriks, T. F. E.; Krestensen, K. K.; Mohren, R.; Vandenbosch, M.; De Vleeschouwer, S.; Heeren, R. M. A.; Cuypers, E. *Analytical Chemistry* **2024**, *96* (10), 4266−4274.

https://doi.org/10.1021/acs.analchem.5c05005
Anal. Chem. XXXX, XXX, XXX−XXX